Ultra-stable graphene aerogels for electromagnetic interference shielding

Journal:	*SCIENCE CHINA Materials*
Manuscript ID	SCMs-2022-0807.R1
Manuscript Type:	Article
Date Submitted by the Author:	27-Jun-2022
Complete List of Authors:	Zhu, Enhui Pang, Kai Chen, Yanru Liu, Senping Liu, Xiaoting Xu, Zhen Liu, Yingjun Gao, Chao; Polymer Science and Engineering
Keywords:	graphene aerogel, mechanical stability, electromagnetic shielding, vacuum bagging, environmental adaptiveness
Speciality:	graphene, graphene aerogel, electromagnetic shielding

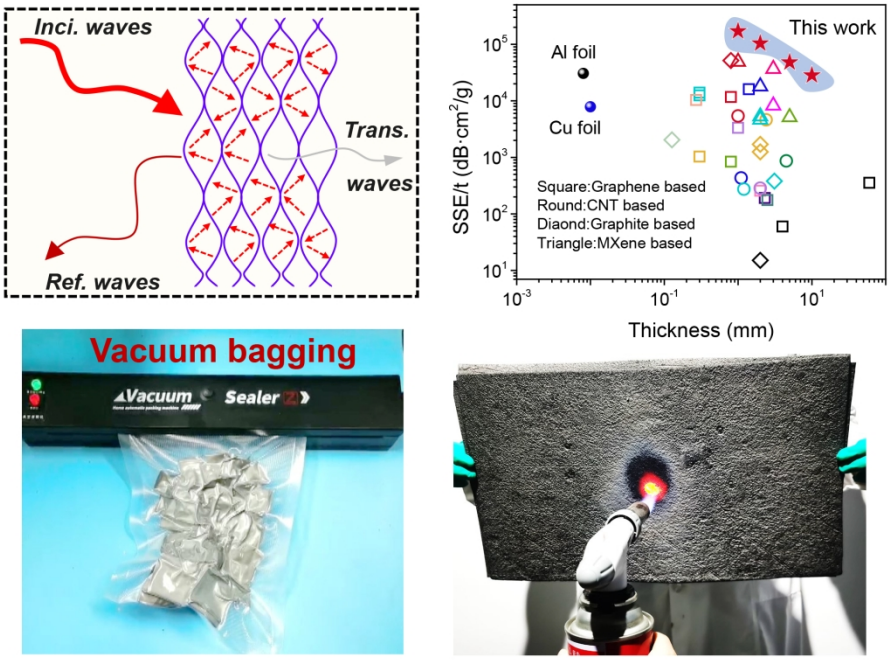

793x540mm (72 x 72 DPI)

SCIENCE CHINA Materials ARTICLES
mater.scichina.com link.springer.com

Ultra-stable graphene aerogels for electromagnetic interference shielding

Enhui Zhu[1], Kai Pang[1*], Yanru Chen[1], Senping Liu[1], Xiaoting Liu[1*], Zhen Xu[1], Yingjun Liu[1,2*], Chao Gao[1*]

ABSTRACT Graphene aerogels (GAs) are prevailing to solve electromagnetic interference (EMI) issues in next-generation electronic devices. However, the practical EMI shielding application of lightweight GAs is still a great challenge because of their structural instability confronted with complex conditions. Here, we report a class of ultra-stable GAs with excellent and reliable EMI shielding performances. The GA (ρ = 3.7 mg/cm^3) with face-to-face stacked structure exhibits a high shielding effectiveness (SE) of 64.1 dB at the thickness of 1 mm. The specific EMI SE reach 173243 dB·cm^2/g, far beyond the previous carbon-based materials. Meanwhile, the structural stability endows the GAs with outstanding resistance to external stimuli, such as mechanical deformation, extreme temperature, flame and underwater environments. The intrinsic conflict of low density and oversized volume is solved by vacuum bagging without structure and performance loss. Our GAs have paved the way to the practical EMI shielding materials and greatly broadened applied scenes, such as aerospace, warcraft and ocean fields.

Keywords: graphene aerogel, mechanical stability, electromagnetic shielding, vacuum bagging, environmental adaptiveness

INTRODUCTION

With the development of electronic devices, electromagnetic interference (EMI) issues inevitably arise, and the superfluous electromagnetic waves (EMWs) may cause the disclosure of information, shorten the lifespan of precision instruments or even affect human health [1-4]. Compared with conventionally easy-corrosive and heavy metal materials, carbon nanomaterials especially two-dimensional graphene [5-8] hold great potential for next-generation EMI shielding materials due to relatively high electrical conductivity and excellent flexibility. In addition to forming a well-defined conductive network, being as lightweight as possible is also a critical demand. Therefore, the highly porous graphene aerogels (GAs) with low density are promising for EMI shielding. However, monolithic GAs suffered from severe deterioration of bulk electrical conductivity because of the extremely diluted connections and weak joints in their porous networks, which hindered the electron transfer in graphene sheets.

Many efforts have been explored to enhance the electrical conductivity and improve the EMI shielding performance of GAs. The prevailing approach is the introduction of other conductive components. Liang et al. have blended silver platelets and graphene oxide (GO) to improve the electrical conductivity of GAs from 0.1 to 45.3 S/m. The corresponding EMI shielding effectiveness (SE) reached ~58 dB at the thickness of 3 mm [9]. Kong et al. introduced 1D CNT to prepare GA composite materials and the EMI SE reached ~36 dB at the thickness of 1.6 mm [10]. Another approach is to regulate the sheets orientation of GAs. Li et al. controlled the spatial distribution of graphene sheets by mechanical compression. The electrical conductivity of GAs increased to 181.8 S/m and EMI SE reached ~43 dB at the thickness of 2.5 mm [11]. The GAs made by directional-freezing method exhibited EMI SE of 32 dB along the radial direction with a slightly decreased shielding effectiveness of 25 dB along the axial direction at the thickness of 4 mm [12]. Despite the electrical conductivity and EMI shielding performance were improved by these strategies, the intrinsically dilute connection of GA still remains and results the poor structural robustness, which greatly limited their practical applications in diversified environments. Therefore, how to fabricate highly conductive GAs with extremely mechanical integrity is still a challenge.

Herein, we proposed a class of ultra-stable GAs within extreme environments with excellent EMI shielding performances. As-prepared GAs hold with higher contact areas by face-to-face connected graphene sheets along the plane direction, which constructed more electron transfer paths and owned with electrical conductivity of 490.2 S/m at density of 3.7 mg/cm^3. By the synergistic effect of excellent conductivity and multiple interfaces, the EMI SE of GAs can reach 64.1 dB at the thickness of 1 mm. As comparison, our GAs possess highest specific EMI SE than

[1]MOE Key Laboratory of Macromolecular Synthesis and Functionalization, Department of Polymer Science and Engineering, Key Laboratory of Adsorption and Separation Materials & Technologies of Zhejiang Province, Zhejiang University, 38 Zheda Road, Hangzhou 310027, China.
[2]Shanxi-Zheda Institute of Advanced Materials and Chemical Engineering, Taiyuan 030032, China.
*Corresponding author (email: pangkai2015@zju.edu.cn (Pang K); xiaotingliu@zju.edu.cn (Liu XT); yingjunliu@zju.edu.cn (Liu YJ); chaogao@zju.edu.cn (Gao C))

other reported lightweight materials. The face-to-face connection endows GAs with outstanding mechanical integrity, which can keep stable and reliable EMI shielding performance in mechanical deformation, extreme temperature, flame and underwater environments. Importantly, our GAs can solve the intrinsic conflict of low density and oversized volume that can be transported by vacuum bagging without structural damage and performance degradation, solving key problems for industrial applications.

EXPERIMENTAL SECTION

Preparation of HGA

Fig. 1a schematically illustrates the fabrication process of GAs by hydroplastic foaming (HPF) [13]. We adopted the GO with typical height of ~1 nm as the raw material (Fig. S1). Firstly, GO suspension (10 mg/ml) was coated on a Teflon plate to fabricate GO film. Then, the GO film was put into hydrazine (30 wt.%) solution to fabricate GO aerogel by HPF. As-prepared GO aerogel was washed by ethanol to remove residual water and hydrazine. Lastly, GO aerogel was chemically reduced under 90 ℃ (hydroiodic acid/acetic acid in a volume ratio of 1:1) for 12 h and annealed at 1600 ℃ for 1 h in a flowing argon atmosphere to obtain hyperbolic graphene aerogels (HGAs).

Characterization

Scanning electron microscope (SEM) images were taken on a Hitachi S4800 field-emission SEM system. The electrical conductivity was measured by source meter (Keithley 2400) using four-probe method. As shown in Fig. S2, silver glue was selected as electrodes and HGA was cut into a cuboid to measure the electrical conductivity. The compressive tests were conducted on a microcomputer control electronic universal testing machine (RGWT-4000-20, REGER, Fig. S3). The compressive direction of HGA was along with face-to-face stacked direction. EMI shielding performances test was taken on a vector network analyzer (ZNB 40, Rohde & Schwarz, Germany) using waveguide method (TT-EMWG-X, 8.2-12.4 GHz, Fig. S4). The HGA was cut to fit the size of the holder (length = 22.86 mm, width = 10.16 mm) and the holders were tightly connected with screws to reduce contact resistance. EMI SE was calculated with those scattering parameters (S_{11}, S_{22}, S_{12}, S_{21}) that obtained by vector network analyzer:

$$R = {S_{11}}^2 = {S_{22}}^2 \quad (1)$$

$$T = {S_{12}}^2 = {S_{21}}^2 \quad (2)$$

$$A = 1 - R - T \quad (3)$$

$$SE_T = -10log_{10}T \quad (4)$$

$$SE_R = -10log_{10}(1 - R) \quad (5)$$

$$SE_A = SE_T - SE_R \quad (6)$$

Where R, T, and A represent reflection, transmission and absorption power coefficient. SE_T, SE_R, and SE_A represent the total, reflective, and absorptive shielding effectiveness, respectively.

RESULTS AND DISCUSSION

We have investigated the structural differences between HGAs and directly annealed graphene film (Fig. 1b and c). The graphene film with 77.28% porosity was fabricated from GO film by chemical reduction and thermal annealing (1600 ℃). The removal of oxygen resulted serious delamination by gas escaping (Fig. 1b). In contrast, HGAs kept hyperbolically connected framework without delamination due to the highly porous channels for gas releasing (Fig. 1c). The surface morphologies of graphene film and HGAs both exhibited dense structures (Fig. 1b and c) with less vertical pores. Therefore, the gas foaming mainly occupied between the graphene sheets without disrupting the oriented structure of intrinsically anisotropic GO films. The graphene blocks of HGAs can be regarded as being sandwiched between two space layers with 3D porous curvatures. The HGAs shows highly ordered and oriented pores that can be controlled by the foaming time from several micrometers to hundreds of micrometers (Fig. S5a-c). The HR-TEM image (Fig. S5d) demonstrated the graphene walls of HGA consisted of ~15 nm carbon layers. The density of HGA and corresponding thickness with foaming time is shown in Fig. S6, and the micro-thick GO film (~20 μm) can be transformed into thick HGAs of ~7.8 mm with extremely low density (3.7 mg/cm^3). From Raman spectra (Fig. S7), D bands at 1350 cm^{-1} (representative of defects in graphite unit) shows nearly the same intensity for graphene film and HGAs with different density, suggesting that the increment of pore size cannot influence the graphene restoration after 1600 ℃ treatment.

The electrical conductivity and EMI shielding performance of HGAs are systematically studied in Fig. 2. As known, the electrical conductivity is a key factor to determine the electromagnetic shielding performance. In general, higher electrical conductivity means more effective EMI shielding effectiveness of materials. Electrical conductivity measurement had been conducted with different thickness, width and length of HGA for a given density and different density for a given thickness to ensure the accuracy (Fig. S8). The electrical conductivity of our HGAs reached 490.2 S/m at the density of 3.7 mg/cm^3 (Fig. 2a), which was lower than graphene films (13000 S/m) at the density of 500 mg/cm^3. However, we found the EMI SE of lightweight HGAs (112.2 dB) is about two times higher than graphene film (60.2 dB), implying ~99.9999999994% incident radiation is blocked and only 0.0000000006% transmittance. The improved EMI shielding performance of HGAs with lower electrical conductivity can be explained by Simon formalism [14]:

$$EMI\ SE = 50 + 10log_{10}\frac{\sigma}{f} + 1.7t(\sigma f)^{0.5} \quad (7)$$

where σ, t, f represents the electrical conductivity, sample

thickness and EMWs frequency, respectively. Besides the electrical conductivity, the sample thickness of HGAs induced by air layers also plays a critical role for EMI shielding. We have also analyzed reflection coefficients (*R*) and absorption coefficients (*A*) of HGAs with different density and thickness (Fig. 2b, Fig. S9). The *R* is higher than *A*, suggesting the reflection is primary shielding mechanisms. Besides, the A increased with the decreased density, indicting the air pores were beneficial to the EMWs' absorption by multiple reflection within pores [15,16]. In general, EMI shielding mechanism can be such expressed: a portion of incident EMWs are directly reflected due to free electrons distributed on the surface and residual EMWs suffered with the dielectric loss including polarization relaxation and energy dissipating [17]. Above process is repeated when EMWs pass through the surface and encounter with the next interface until completely disappeared. As comparison, the reflection shielding of graphene film dominates by impedance mismatch and tightly interlayer bonding (Fig. 2c), however, the dielectric loss can be promoted additionally in HGA because of wider propagation paths and multiple interfaces within air pores [18]. We think the anisotropic pores and consecutively conductive pathways in HGA should be responsible for the enhanced EMI shielding performance. Moreover, we have employed the GO with different thickness and aspect ratio as raw materials to fabricated HGAs. As shown in Fig. S10, the giant and single-layered GO can endow the HGAs with higher electrical conductivity and EMI SE because of less electron trapping sites and sheets aggregation [19,20].

All HGAs samples were cut into 1 mm to conduct EMI shielding tests in *X* bands (Fig. 2d) at different density. When the density decreased from 13.0 mg/cm^3 to 3.7 mg/cm^3, the EMI SE exhibits descending trend from 98.7 to 64.1 dB own to less internal interfaces and free electrons. To further evaluate the EMI shielding performance, we have introduced the specific shielding effectiveness which is divided by thickness (SSE/t) as a general standard to normalize the effect of density and thickness. From Fig. 2e, our HGAs exhibits superb SSE/t of 173243 dB • cm^2/g at the thickness of 1 mm (3.7 mg/cm^3), ranking at the top of the carbon-based materials including graphite, graphene, MXene and CNT [21-52]. Moreover, the EMI SE of HGAs can also exceed the other reported carbon-based porous materials and composites (Table S1), exhibiting great practical application values.

The HGAs possess excellent mechanical stability, which is the prerequisite for the practical application. The compressive curves of HGA (Fig. S11) shows that the HGA always kept stable during fatigue cycles and can easily recover to its original state. The stress remaining and plastic deformation during compressions at an extreme deformation of 95% were exhibited in Fig. 3a. The HGA retains 60% of the maximum stress and the plastic deformation is only 5% after 10000-cycles compression, which is difficult to be achieved in GAs by conventional freeze drying and chemical vapor deposition methods. The energy loss coefficient was about 50% during compressive tests.It should be noticed that the EMI SE is stable and maintain with high level during compressive cycles (Fig. 4b), suggesting the reflective interfaces and inner structures of HGA were not damaged during cycling compression. Besides, we demonstrated the GAs after 1600℃ treatment possess better EMI shielding performance and compressive resilience than those after 300, 600, 900 and 1200℃ treatment, which attributed by the structural restoration of graphene at higher temperature (Fig. S12).

For the commercial conductive polymer composites, the stress relaxation is the intrinsic weakness due to the slippage of polymer molecules. Therefore, we have investigated the stress relaxation behaviors of HGAs at 99% strain for 30 days (Fig. 3c). HGA presents negligible stress loss in 30 days as well as EMI SE (Fig. 3d), exhibiting the overwhelming mechanical stability than the most commercial EMI shielding materials. The HGAs owned with small Poisson's ratio (~0.08, Fig. S13), indicating the compressive loads can be dispersed by inner wrinkles on hyperbolic graphene sheets rather than the transverse bulging. We think the excellent mechanical performances of HGAs were originated by the hyperbolic structures with positive Gaussian curvatures of graphene walls that can easily sustain with external loads by stress distribution along the dimensions of surface curvature to avoid bending stress concentration and structural damage.

For the most of lightweight aerogels, the low density and large volume are the intrinsic conflicts. HGA materials with high porosity (above 95%) fills the gap by providing a vacuum bagging method. The superior flexibility of HGAs (Fig. S14) is the precondition for vacuum bagging. Firstly, many HGAs monoliths (bulk volume of ~240 cm^3) were stacked into a PVC vacuum bag (the left of Fig. 4a) and then a vacuum sealer (with vacuum pressure of 70 kPa) was employed to extrude the extra air in vacuum bag for 1 min. After extrusion process, the vacuum bag with HGAs samples was sealed with hot laminating by vacuum sealer, which owned with limited volume of ~20 cm^3 (the middle of Fig. 4a). Finally, the bag with negative pressure was tore at normal pressure which can achieve the air inflation spontaneously, and the inflated HGAs monoliths can easily recover to initial shape (the right of Fig. 4a). The detailed process can be seen in Movie S1. In the middle picture of Fig. 4a, we can see that the HGAs were suffering with complex deformations, such as bending, folding, tearing and tension, exhibited the excellent structural stability to withstand three-dimensional deformations. Moreover, those HGAs still keep high and stable EMI SE after 10-cycles vacuum bagging processes (Fig. 4b). These characteristics ensure the HGAs can be easily packed and transported in practical applications.

For EMI shielding applications especially in building trades, the environmental adaptiveness of shielding materials is an important parameter. We have demonstrated the HGAs showed extreme stability within harsh condition (Fig. 5). The HGA displays excellent flame-retardant in burning process with little residual carbon production on the surface (Fig. 5a). Fig. 5b shows the thermal infrared image of the HGA. The color of the area above the HGA is blue rather than red, indicating its ability to suppress

radiation. In general, conduction and radiation heat transfer are the key factors for thermal conductivity [53]. The high porosity HGA that fills with air is believed to hinder thermal radiation. Meanwhile, the EMI SE of HGA only keeps minimal reduction at the initial stages and then holds stable. These flame-retardant properties of EMI shielding materials can provide great security for the human and facility.

Moreover, we also evaluated the total EMI SE of HGA after extreme treatment at 400 ℃ (air environment) and -196 ℃ (liquid nitrogen), which can keep nearly unchanged (Fig. 5c). Beyond the high stability at extreme temperatures, the HGA shows negligible variation of EMI SE after compression in water (Fig. 5d). It still possesses great resilience during the repeated water squeezing and keep reliable EMI shielding performance. The extremely environmental adaptiveness of HGAs can provide the all-round protection and increase their economic values in EMI shielding applications.

CONCLUSION

In summary, we have fabricated an ultra-stable HGA with excellent EMI shielding performance which can reach 64.1 dB at the thickness of 1 mm and density of 3.7 mg/cm^3. The specific shielding effectiveness reached up to 173243 dB·cm^2/g, which is the highest among previous lightweight carbon-based materials. As-prepared HGAs exhibited excellent mechanical stability, kept stable EMI shielding performance during 10000-cycles and long-term (30 days) compression. Benefiting from the face-to-face connection of graphene, the HGAs can be easily packed by vacuum bagging without the loss of EMI SE, indicating their excellently mechanical integrity to confront with complex deformations. Even in some extreme environments, the HGAs can operate stably for EMI shielding. Our HGAs can satisfy most of the demands in EMI shielding fields and their stability exhibits great potential in the practical uses for civil, military and national defense.

Received xx-xx 2015; accepted xx-xx 2015;
Published online xx-xx 2015

1 Chen Y, Zhang HB, Yang YB, *et al.* High-performance epoxy nanocomposites reinforced with three-dimensional carbon nanotube sponge for electromagnetic interference shielding. Adv Funct Mater, 2016, 26: 447-455.
2 Shu JC, Cao WQ, Cao MS. Diverse metal-organic framework architectures for electromagnetic absorbers and shielding. Adv Funct Mater, 2021, 31: 2100470.
3 Huang Y, Li N, Ma Y, *et al.* The influence of single-walled carbon nanotube structure on the electromagnetic interference shielding efficiency of its epoxy composites. Carbon, 2007, 45: 1614-1621.
4 He P, Cao MS, Cao WQ, *et al.* Developing MXenes from wireless communication to electromagnetic attenuation. Nanomicro Lett, 2021, 13: 1-34.
5 Huang ZY, Chen HH, Huang Y, *et al.* Ultra-broadband wide-angle terahertz absorption properties of 3D graphene foam. Adv Funct Mater, 2018, 28: 1704363.
6 Zhang Y, Huang Y, Zhang TF, *et al.* Broadband and tunable high-performance microwave absorption of an ultralight and highly compressible graphene foam. Adv Mater, 2015, 27: 2049-2053.
7 Liang JJ, Wang Y, Huang Y, *et al.* Electromagnetic interference shielding of graphene/epoxy composites. Carbon, 2009, 47: 922-925.
8 Chen Z, Xu C, Ma C, *et al.* Lightweight and flexible graphene foam composites for high-performance electromagnetic interference shielding. Adv Mater, 2013, 25: 1296-1300.
9 Liang C, Song P, Qiu H, *et al.* Constructing interconnected spherical hollow conductive networks in silver platelets/reduced graphene oxide foam/epoxy nanocomposites for superior electromagnetic interference shielding effectiveness. Nanoscale, 2019, 11: 22590-22598.
10 Kong L, Yin X, Han M, *et al.* Macroscopic bioinspired graphene sponge modified with in-situ grown carbon nanowires and its electromagnetic properties. Carbon, 2017, 111: 94-102.
11 Li CB, Li YJ, Zhao Q, *et al.* Electromagnetic interference shielding of graphene aerogel with layered microstructure fabricated via mechanical compression. ACS Appl Mater Interfaces, 2020, 12: 30686-30694.
12 Li XH, Li X, Liao KN, *et al.* Thermally annealed anisotropic graphene aerogels and their electrically conductive epoxy composites with excellent electromagnetic interference shielding efficiencies. ACS Appl. Mater. Interfaces 2016, 8: 33230-33239.
13 Pang K, Song X, Xu Z, *et al.* Hydroplastic foaming of graphene aerogels and artificially intelligent tactile sensors. Sci Adv, 2020, 6: abd4045.
14 Das NC, Liu Y, Yang K, *et al.* Single-walled carbon nanotube/poly (methyl methacrylate) composites for electromagnetic interference shielding. Polym Eng Sci, 2009, 49: 1627-1634.
15 Cao MS, Shu JC, Wen B, *et al.* Genetic dielectric genes inside 2D carbon-based materials with tunable electromagnetic function at elevated temperature. Small Structures, 2021, 2(11): 2100104.
16 Wang XX, Shu JC, Cao WQ, *et al.* Eco-mimetic nanoarchitecture for green EMI shielding. Chem Eng J, 2019, 369: 1068-1077.
17 Xi J, Li Y, Zhou E, *et al.* Graphene aerogel films with expansion enhancement effect of high-performance electromagnetic interference shielding. Carbon, 2018, 135: 44-51.
18 Wan YJ, Zhu PL, Yu SH, *et al.* Anticorrosive, ultralight, and flexible carbon-wrapped metallic nanowire hybrid sponges for highly efficient electromagnetic interference shielding. Small, 2018, 14: e1800534.
19 Wen B, Cao MS, Lu MM, *et al.* Reduced graphene oxides: light-weight and high-efficiency electromagnetic interference shielding at elevated temperatures. Adv Mater, 2014, 26(21): 3484-3489.
20 Fang XY, Yu XX, Zheng HM, *et al.* Temperature-and thickness-dependent electrical conductivity of few-layer graphene and graphene nanosheets. Phys Lett A, 2015, 379(37): 2245-2251.
21 Song WL, Guan XT, Fan LZ, *et al.* Tuning three-dimensional textures with graphene aerogels for ultra-light flexible graphene/texture composites of effective electromagnetic shielding. Carbon, 2015, 93: 151-160.
22 Bi S, Zhang L, Mu C, *et al.* Electromagnetic interference shielding properties and mechanisms of chemically reduced graphene aerogels. Appl Surf Sci, 2017, 412: 529-536.
23 Paliotta L, Bellis GD, Tamburrano A, *et al.* Highly conductive multilayer-graphene paper as a flexible lightweight electromagnetic shield. Carbon, 2015, 89: 260-271.
24 Agnihotri N, Chakrabarti K, De A. Highly efficient electromagnetic interference shielding using graphite nanoplatelet/poly (3,4-ethylenedioxythiophene)-poly (styrenesulfonate) composites with enhanced thermal conductivity. RSC Adv, 2015, 5: 43765-43771.
25 Song WL, Guan XT, Fan LZ, *et al.* Magnetic and conductive graphene papers toward thin layers of effective electromagnetic shielding, J Mater Chem A, 2015, 3: 2097-2107.
26 Pande S, Chaudhary A, Patel D, *et al.* Mechanical and electrical properties of multiwall carbon nanotube/polycarbonate composites for electrostatic discharge and electromagnetic interference shielding applications. RSC Adv, 2014, 4: 13839-13849.

27 Al-Saleh MH, Saadeh WH, Sundararaj U. EMI shielding effectiveness of carbon based nanostructured polymeric materials: A comparative study. Carbon, 2013, 60: 146-156.
28 Arjmand M, Apperley T, Okoniewski M, *et al.* Comparative study of electromagnetic interference shielding properties of injection molded versus compression molded multi-walled carbon nanotube/polystyrene composites. Carbon, 2012, 50: 5126-5134.
29 Ling J, Zhai W, Feng W, *et al.* Facile preparation of lightweight microcellular polyetherimide/graphene composite foams for electromagnetic interference shielding. ACS Appl Mater Interfaces, 2013, 5: 2677-2684.
30 Yan DX, Ren PG, Pang H, *et al.* Efficient electromagnetic interference shielding of lightweight graphene/polystyrene composite. J Mater Chem, 2012, 22: 18772-18774.
31 Zhang HB, Yan Q, Zheng WG, *et al.* Tough graphene-polymer microcellular foams for electromagnetic interference shielding. ACS Appl Mater Interfaces, 2011, 3: 918-924.
32 Shen B, Li Y, Yi D, *et al.* Microcellular graphene foam for improved broadband electromagnetic interference shielding. Carbon, 2016, 102: 154-160.
33 Shen B, Zhai W, Tao M, *et al.* Lightweight, multifunctional polyetherimide/graphene@Fe_3O_4 composite foams for shielding of electromagnetic pollution. ACS Appl Mater Interfaces, 2013, 5: 11383-11391.
34 Li Y, Shen B, Pei X, *et al.* Ultrathin carbon foams for effective electromagnetic interference shielding. Carbon, 2016, 100: 375-385.
35 Zeng Z, Jin H, Chen M, *et al.* Lightweight and anisotropic porous MWCNT/WPU composites for ultrahigh performance electromagnetic interference shielding. Adv Funct Mater, 2016, 26: 303-310.
36 Zhang L, Liu M, Roy S, *et al.* Phthalonitrile-based carbon foam with high specific mechanical strength and superior electromagnetic interference shielding performance. ACS Appl Mater Interfaces, 2016, 8: 7422-7430.
37 Song WL, Wang J, Fan LZ, *et al.* Interfacial engineering of carbon nanofiber-graphene-carbon nanofiber heterojunctions in flexible lightweight electromagnetic shielding networks. ACS Appl Mater Interfaces, 2014, 6: 10516-10523.
38 Moglie F, Micheli D, Laurenzi S, *et al.* Electromagnetic shielding performance of carbon foams. Carbon, 2012, 50: 1972-1980.
39 Xu H, Yin X, Li X, *et al.* Lightweight $Ti_3C_2T_x$ MXene/poly (vinyl alcohol) composite foams for electromagnetic wave shielding with absorption-dominated feature. ACS Appl Mater Interfaces, 2019, 11: 10198-10207.
40 Han M, Yin X, Hantanasirisakul K, *et al.* Anisotropic Mxene aerogels with a mechanically tunable ratio of electromagnetic wave reflection to absorption. Adv Opt Mater, 2019, 7: 1900267.
41 Liu J, Zhang HB, Sun R, *et al.* Hydrophobic, flexible, and lightweight MXene foams for high-performance electromagnetic-interference shielding. Adv Mater, 2017, 29: 1702367.
42 Zhou Z, Liu J, Zhang X, *et al.* Ultrathin MXene/calcium alginate aerogel film for high-performance electromagnetic interference shielding. Adv Mater Interfaces, 2019, 6: 1802040.
43 Zhao S, Zhang HB, Luo JQ, *et al.* Highly electrically conductive three-dimensional $Ti_3C_2T_x$ MXene/reduced graphene oxide hybrid aerogels with excellent electromagnetic interference shielding performances. ACS Nano, 2018, 12: 11193-11202.
44 Sambyal P, Iqbal A, Hong J, *et al.* Ultralight and mechanically robust $Ti_3C_2T_x$ hybrid aerogel reinforced by carbon nanotubes for electromagnetic interference shielding. ACS Appl Mater Interfaces, 2019, 11: 38046-38054.
45 Bian R, He G, Zhi W, *et al.* Ultralight MXene-based aerogels with high electromagnetic interference shielding performance. J Mater Chem C, 2019, 7: 474-478.
46 Wu X, Han B, Zhang HB, *et al.* Compressible, durable and conductive polydimethylsiloxane-coated MXene foams for high-performance electromagnetic interference shielding. Chem Eng J, 2020, 381: 122622.
47 Wei Q, Pei S, Qian X, *et al.* Superhigh electromagnetic interference shielding of ultrathin aligned pristine graphene nanosheets film. Adv Mater 2020, 32: 1907411.
48 Qi FQ, Wang L, Zhang YL, *et al.* Robust $Ti_3C_2T_x$ MXene/starch derived carbon foam composites for superior EMI shielding and thermal insulation. Mater Today Phys, 2021, 21: 100512.
49 Zhang LY, Ruan KP, Shi XT, *et al.* $Ti_3C_2T_x$ /rGO porous composite films with superior electromagnetic interference shielding performances. Carbon, 2021, 175: 271-280.
50 Qian KP, Zhou QF, Wu HM, *et al.* Carbonized cellulose microsphere@void@MXene composite films with egg-box structure for electromagnetic interference shielding. Compos Part A, 2021, 141: 106229.
51 Qian KP, Wu HM, Fang JH, *et al.* Yarn-ball-shaped CNF/MWCNT microspheres intercalating $Ti_3C_2T_x$ MXene for electromagnetic interference shielding films. Carbohydr Polym, 2021, 254: 117325.
52 Qian KP, Li S, Fang JH, *et al.* C60 intercalating $Ti_3C_2T_x$ MXenes assisted by γ-cyclodextrin for electromagnetic interference shielding films with high stability. J Mater Sci Technol, 2022, 127: 71-77.
53 Zhu SQ, Shu JC, Cao MS, *et al.* Novel MOF-derived 3D hierarchical needlelike array architecture with excellent EMI shielding, thermal insulation and supercapacitor performance. Nanoscale, 2022, 14(19): 7322-7331.

Acknowledgements Funding: This work is supported by MOE Key Laboratory of Macromolecular Synthesis and Functionalization, International Research Center for X Polymers, the National Natural Science Foundation of China (Nos. 51973191, 52090030), Shanxi-Zheda Institute of New Materials and Chemical Engineering (No. 2012SZ-FR004), Hundred Talents Program of Zhejiang University (188020*194231701/113), Fujian Provincial Science and Technology Major Projects (NO. 2018HZ0001-2), the Fundamental Research Funds for the Central Universities (Nos. K20200060 and 2021FZZX001-17), Key Laboratory of Novel Adsorption and Separation Materials and Application Technology of Zhejiang Province (512301-I21502), China Postdoctoral Science Foundation (2021M702788), Postdoctoral Research Program of Zhejiang Province (ZJ2021145) and Devices of the Ministry of Education NJ2020003 (INMD-2021M06).

Author contributions Zhu E and Pang K are the co-first author in this work. Pang K, Liu X, Liu Y and Gao C conceived the research. Pang K and Zhu E designed the experiments and analyzed the data. Zhu E, Chen Y and Liu S did the materials characterization and the electromagnetic shielding tests. Zhu E and Liu X wrote the manuscript and all authors provided feedback.

Conflict of interest The authors declare that they have no conflict of interest.

Supplementary information Experimental details and supporting data are available in the online version of the paper.

Enhui Zhu is currently a master candidate at the School of department of polymer science and engineer, Zhejiang University. His current research focuses on electromagnetic shielding applications of graphene materials.

Kai Pang received his Ph. D degree from Zhejiang University in 2021. He is currently a postdoctoral research fellow at Zhejiang University. His research interests include graphene macroscopic assemblies and flexible electronics.

Xiaoting Liu received her Ph. D degree from Zhejiang University in 2020. She is currently a postdoctoral research fellow at Zhejiang University. Her research interests include preparation and application of graphene composites

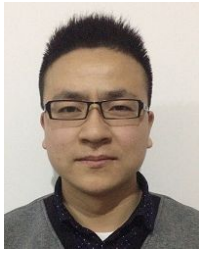

Yingjun Liu received his Ph. D degree from Zhejiang University in 2017. He is currently an assistant research fellow at Zhejiang University. His research interests include high-performance graphene fiber and film.

Chao Gao obtained his Ph.D. degree from Shanghai Jiao Tong University (SJTU) in 2001. He was appointed as an Associate Professor at SJTU in 2002. He did postdoctoral research at the University of Sussex with Prof. Sir Harry W. Kroto and AvH research at the Bayreuth University with Prof. Axel H. E. Müller during 2003-2006. He joined the Department of Polymer Science and Engineering, Zhejiang University in 2008 and was promoted as a full Professor. His research interests focus on graphene chemistry, macroscopic assembly, and energy storage.

超稳定石墨烯气凝胶的电磁屏蔽性能研究

朱恩惠[1]，庞凯[1*]，陈彦儒[1]，刘森坪[1]，刘晓婷[1*]，许震[1]，刘英军[1,2*]，高超[1*]

摘要 石墨烯气凝胶（GAs）在解决下一代电子器件电磁屏蔽污染方面引起了广泛关注。但是，由于超轻石墨烯气凝胶在复杂环境中结构不稳定，其在电磁屏蔽的实际应用中仍存在巨大的挑战。在此，我们提出一类机械结构稳定的石墨烯气凝胶，且展示出优异可靠的电磁屏蔽性能。这类气凝胶呈现出面面堆叠的结构，在密度ρ = 3.7 mg/cm^3，高度1 mm时，电磁屏蔽效能可达到64.1 dB，比电磁屏蔽效能达到173243 dB·cm^2/g，远超现有报道的碳基材料。同时，石墨烯气凝胶具有优异的环境适应性，在机械形变、极端温度、燃烧及水下等环境中均可保持性能稳定。此外，制备的石墨烯气凝胶可通过真空袋装工艺进行包装运输，解决了超轻材料实际应用中低密度与大体积的矛盾，且在这一极端变形过程中材料结构和性能均未产生破坏。该研究为石墨烯气凝胶电磁屏蔽材料的实际应用铺平了道路，且拓展了其实际应用场景，比如航天、军事战机及海洋领域。

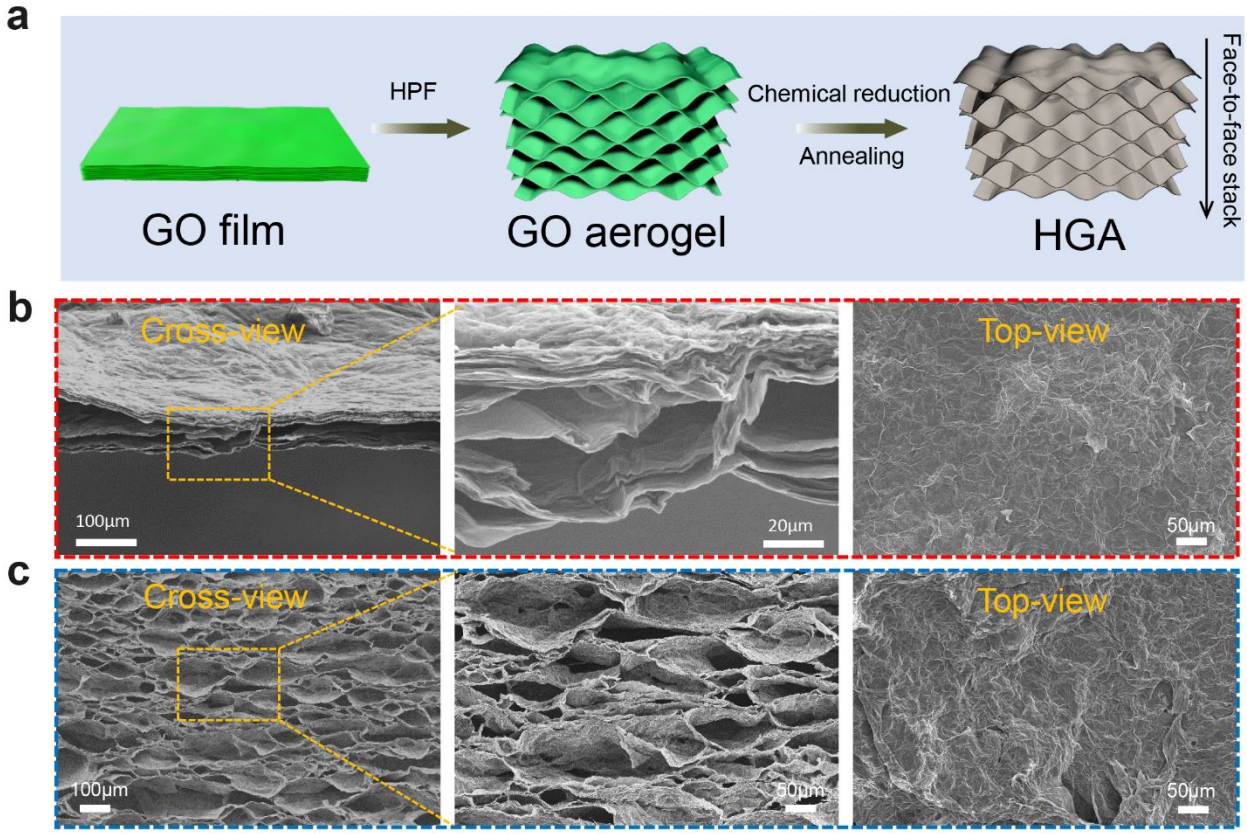

Figure 1 (a) Schematic illustration of fabrication processes of HGA. Cross-section view and top-view SEM images of graphene film (b) and HGA (c).

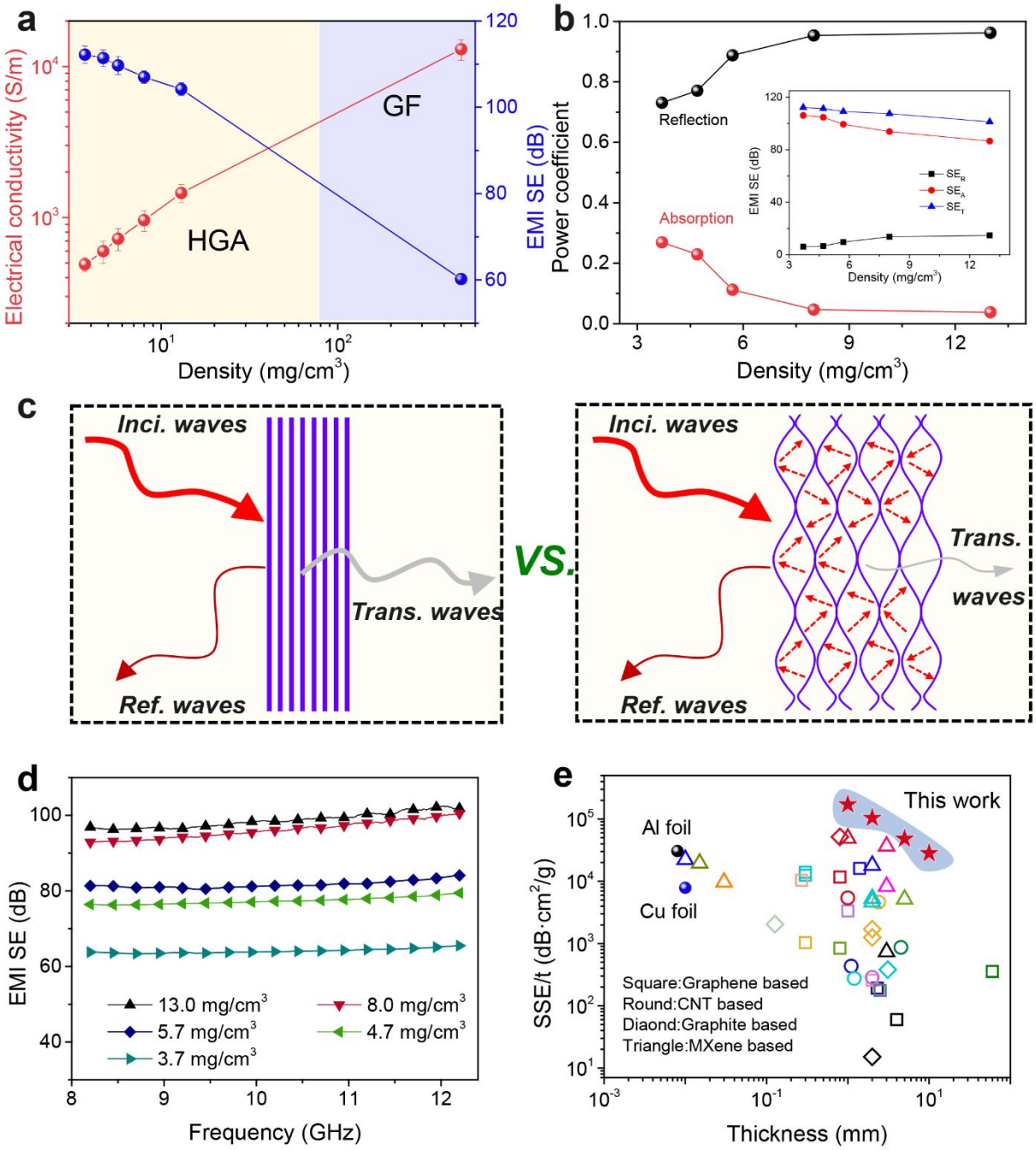

Figure 2 (a) Electrical conductivity and EMI SE at *X*-band of graphene film and HGAs. (b) R, A, SER, SEA, SET of HGAs with different density. (c) Comparison of electromagnetic shielding mechanism for graphene film and HGA. (d) EMI SE of HGAs in *X*-band at the thickness of 1 mm. (e) Comparison of SSE/t of HGAs with other reported EMI shielding materials.

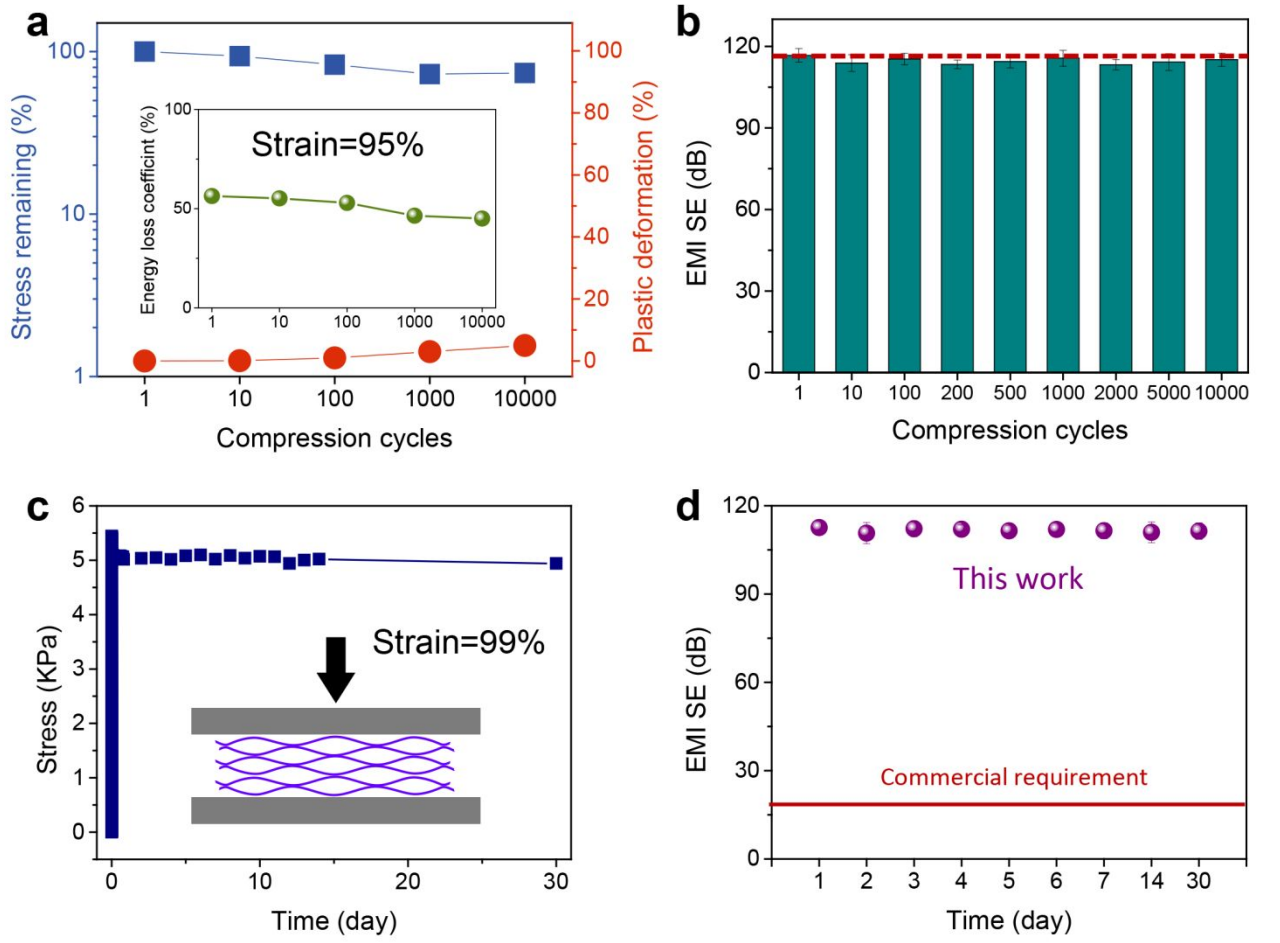

Figure 3 (a) Stress remaining, plastic deformation and energy loss coefficient during 10000-cycles compressive test at 95 % strain of HGA with density of 3.7 mg/cm^3 (b) EMI SE of HGA at *X* band during compressive cycles. (c) Stress relaxation curve of HGA with 99% strain for 30 days. (d) EMI SE of HGA at *X* band during long-term stress relaxation.

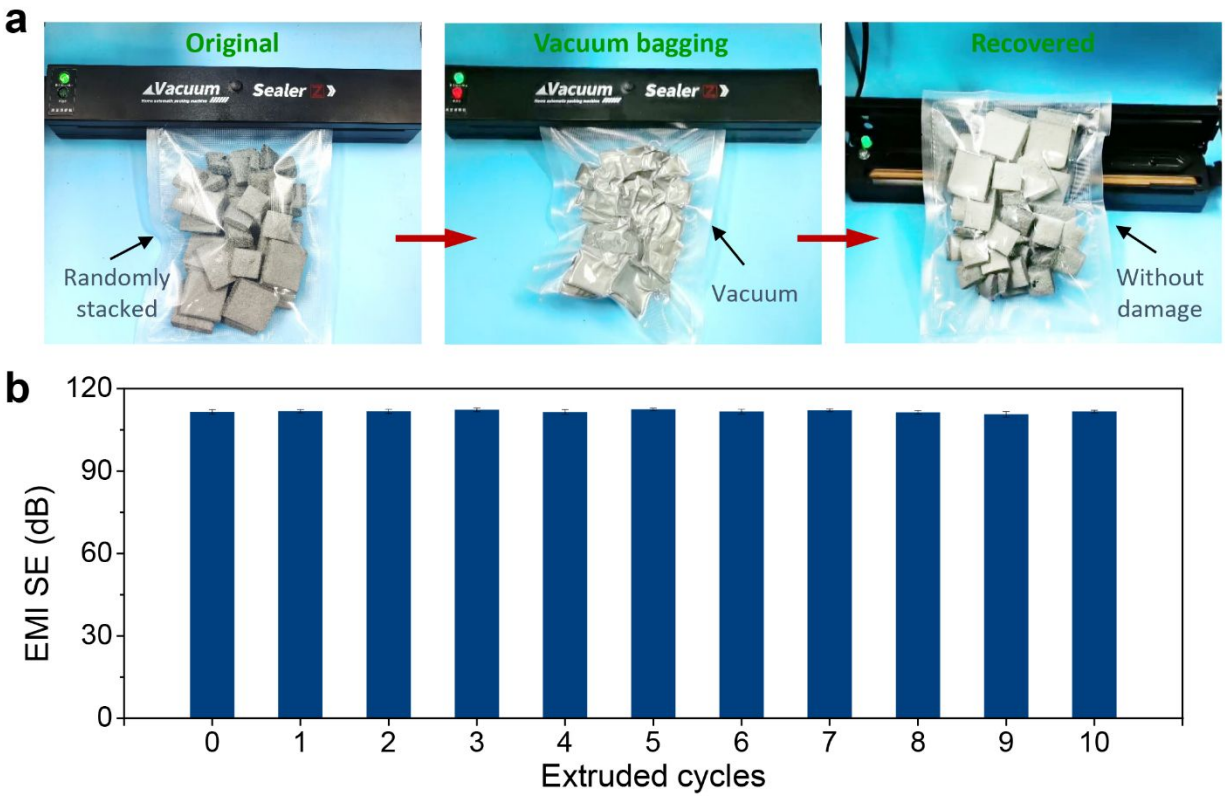

Figure 4 (a) Digital cameras image of HGA during vacuum bagging. (b) EMI SE of HGA at *X* bands after vacuum bagging repeatedly.

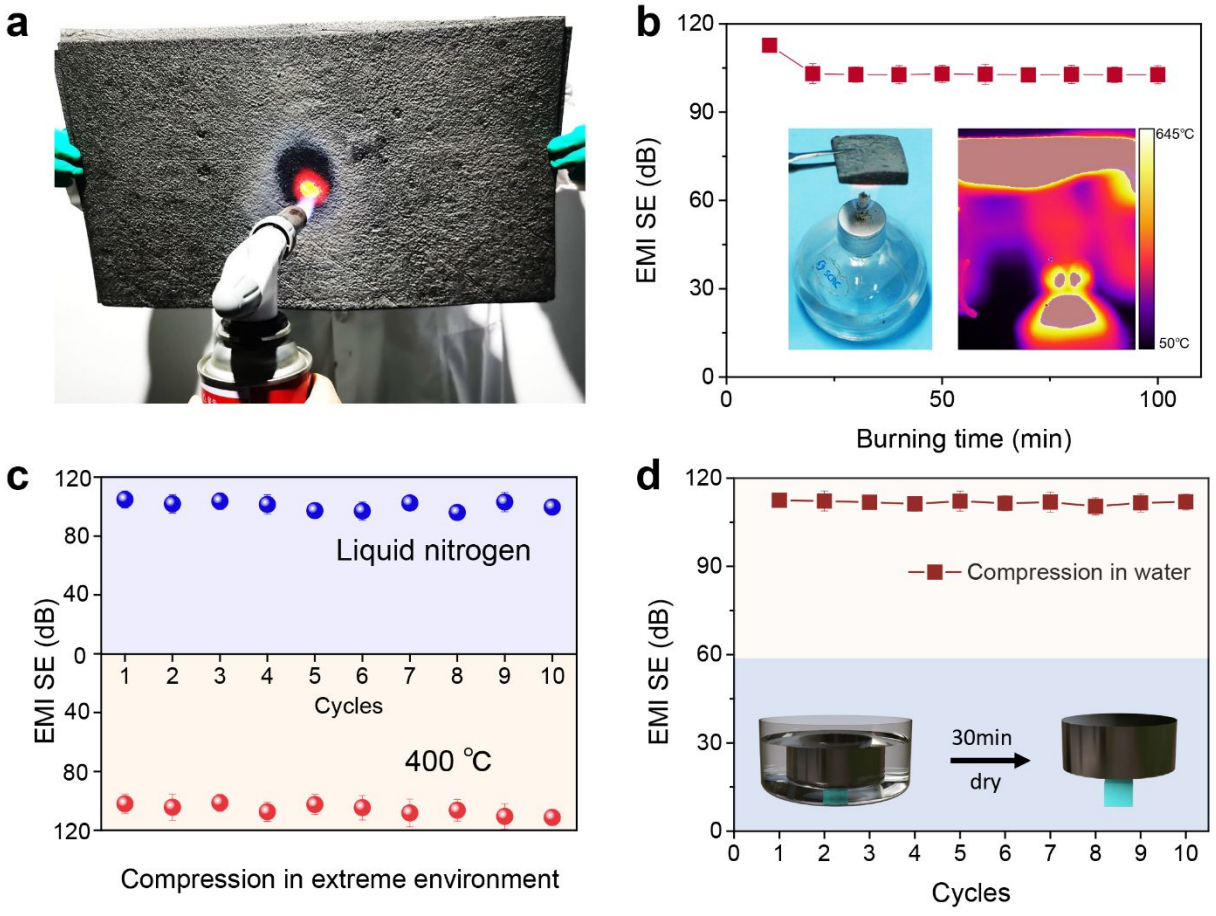

Figure 5 (a) Digital image of HGA to confront with flame. (b) EMI SE of HGA at *X* bands after 2 h flame burning. The insets are the digital image and its infrared picture. (c) EMI SE of HGA at *X* bands after compression in extreme temperature (liquid nitrogen and 400℃ heating). (d) EMI SE of HGA at *X* bands after multiple compression in water.

Supplementary Information

Ultra-stable graphene aerogels for electromagnetic interference shielding

Enhui Zhu[1], Kai Pang[1*], Yanru Chen[1], Senping Liu[1], Xiaoting Liu[1*], Zhen Xu[1], Yingjun Liu[1,2*], Chao Gao[1*]

[1]MOE Key Laboratory of Macromolecular Synthesis and Functionalization, Department of Polymer Science and Engineering, Key Laboratory of Adsorption and Separation Materials & Technologies of Zhejiang Province, Zhejiang University, 38 Zheda Road, Hangzhou 310027, China.

[2]Shanxi-Zheda Institute of Advanced Materials and Chemical Engineering, Taiyuan 030032, China.

[*]Corresponding author (email: pangkai2015@zju.edu.cn (Pang K); xiaotingliu@zju.edu.cn (Liu XT); yingjunliu@zju.edu.cn (Liu YJ); chaogao@zju.edu.cn (Gao C))

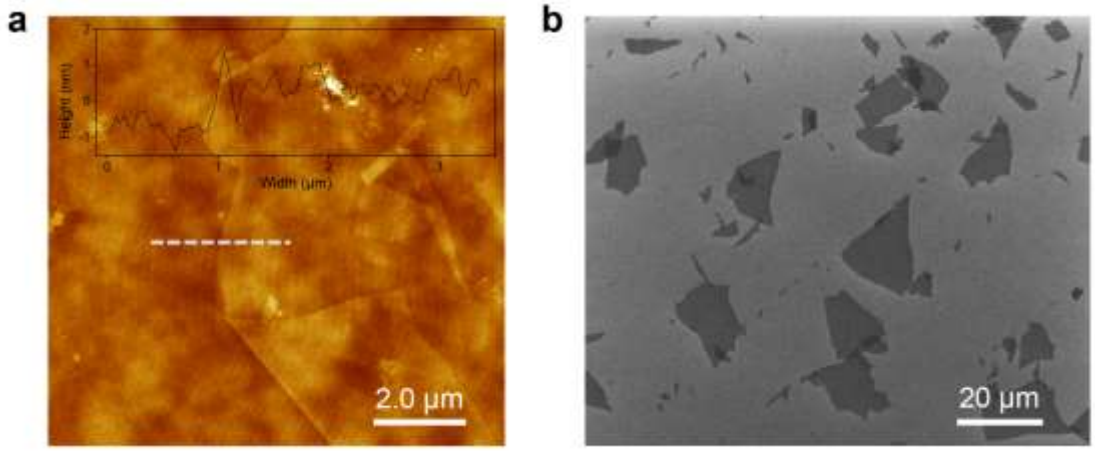

Figure S1 (a) Atomic force microscope image and height profile of GO sheet. (b) SEM image of GO sheets.

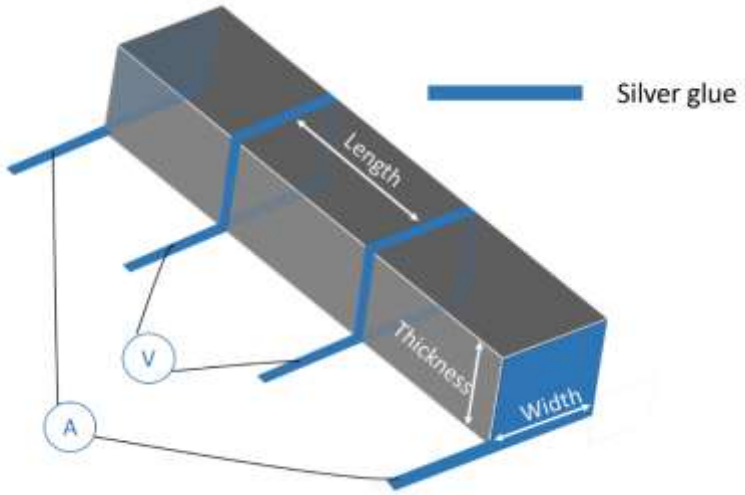

Figure S2 The drawing of electrical conductivity test.

Figure S3 Digital camera image of compression machine.

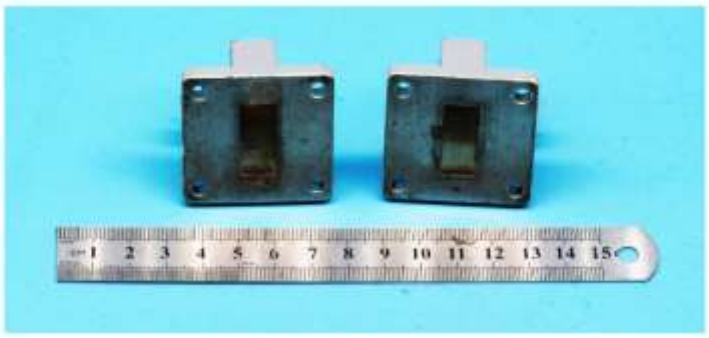

Figure S4 Digital camera image of TT-EMWG-X waveguide holder.

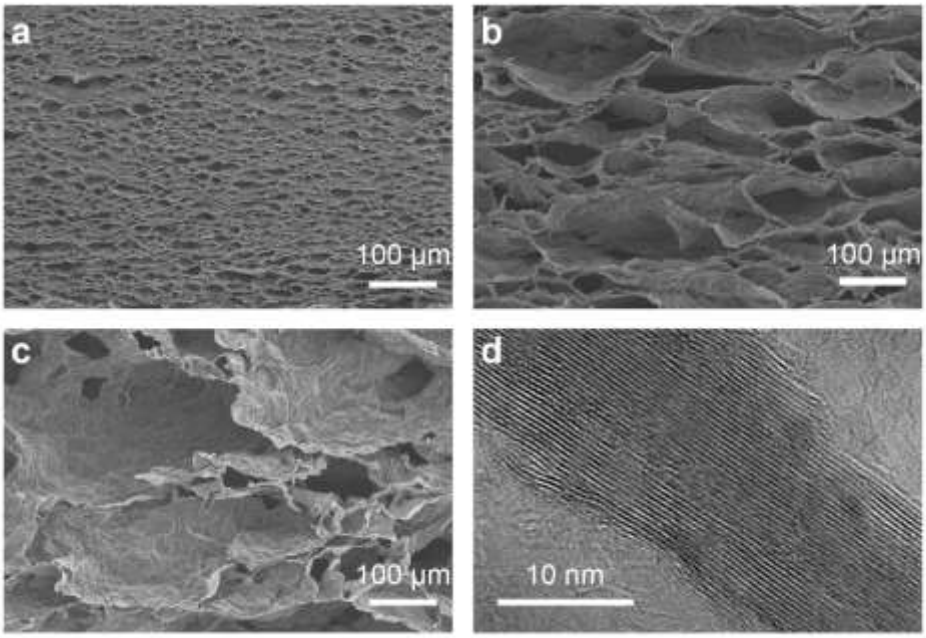

Figure S5 (a-c) Cross-section view SEM image of HGAs from high density to low density. (d) TEM image of HGAs with density of 3.7 mg/cm^3.

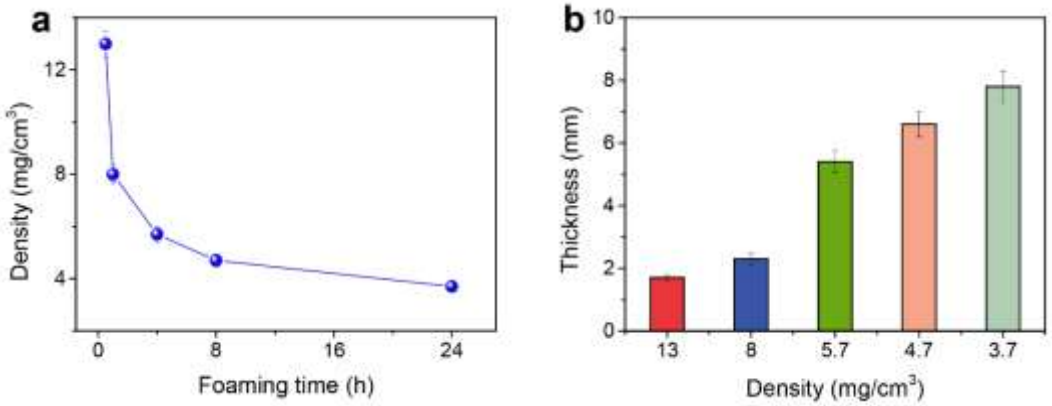

Figure S6 (a) The relationship of density of HGA with foaming time. (b) The thickness of HGA of different density.

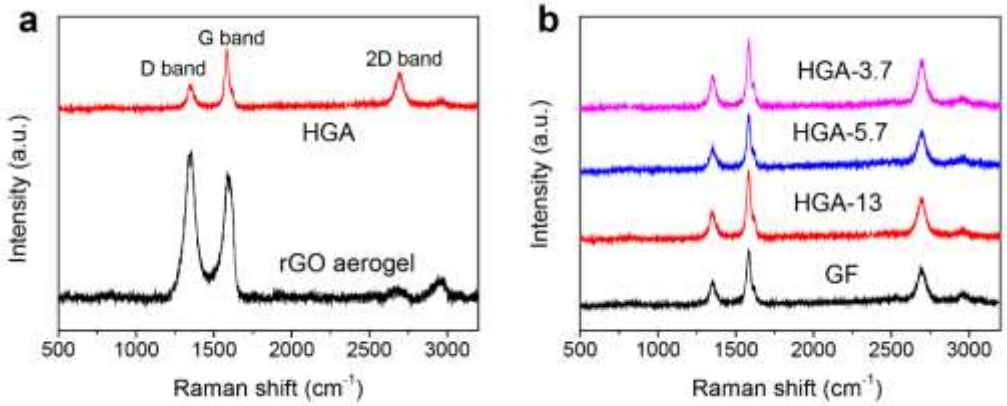

Figure S7 (a) The Raman spectra of HGA and rGO aerogel. (b) The Raman spectra of HGA with different density and graphene film (GF).

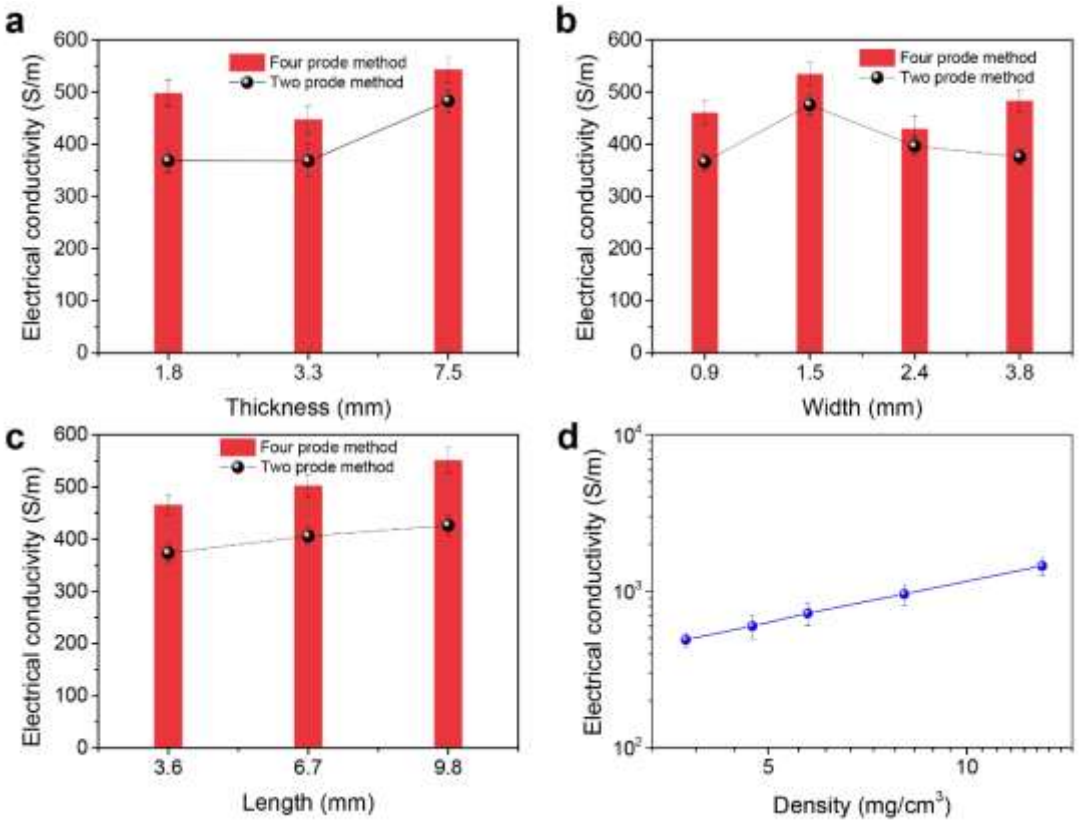

Figure S8 (a-c) The electrical conductivity of HGA measured by different thickness, width and length at 3.7 mg/cm3. (d) The electrical conductivity of HGA at different density at the thickness of 1 mm.

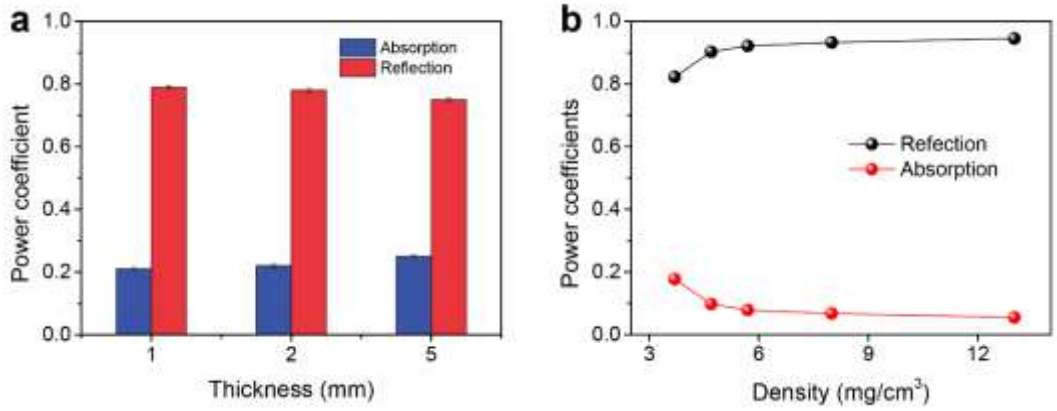

Figure S9 (a) The power coefficient of HGA with different thickness at 3.7 mg/cm3. (b) The power coefficient of HGA with different density at the thickness of 1 mm.

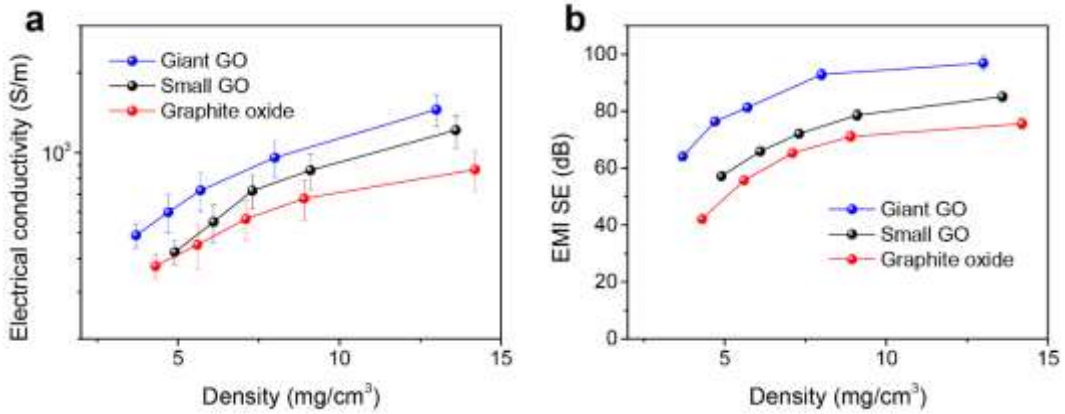

Figure S10 Electrical conductivity (a) and EMI SE at *X* band in the same thickness (b) of HGA prepared by graphite oxide, small GO and giant GO.

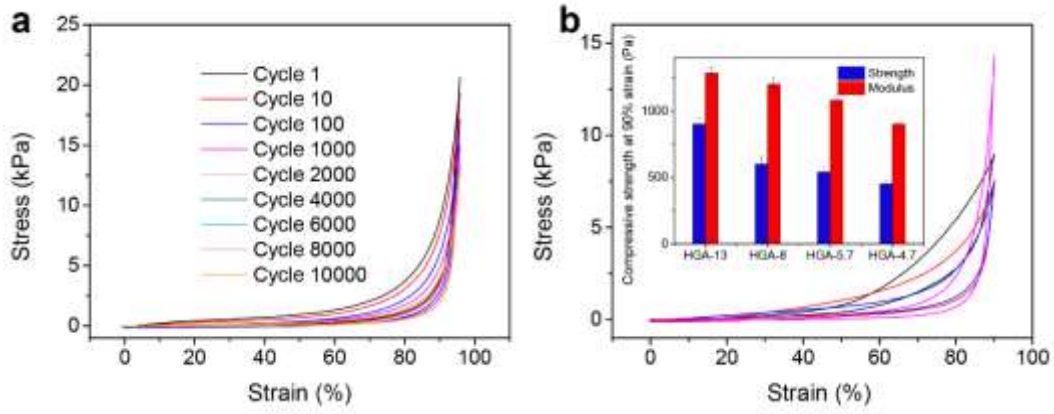

Figure S11 (a) Stress-strain curve of HGA at the density of 3.7 mg/cm^3. (b) Stress-strain curve of HGA of different density. Internal image shows corresponding strength and modulus.

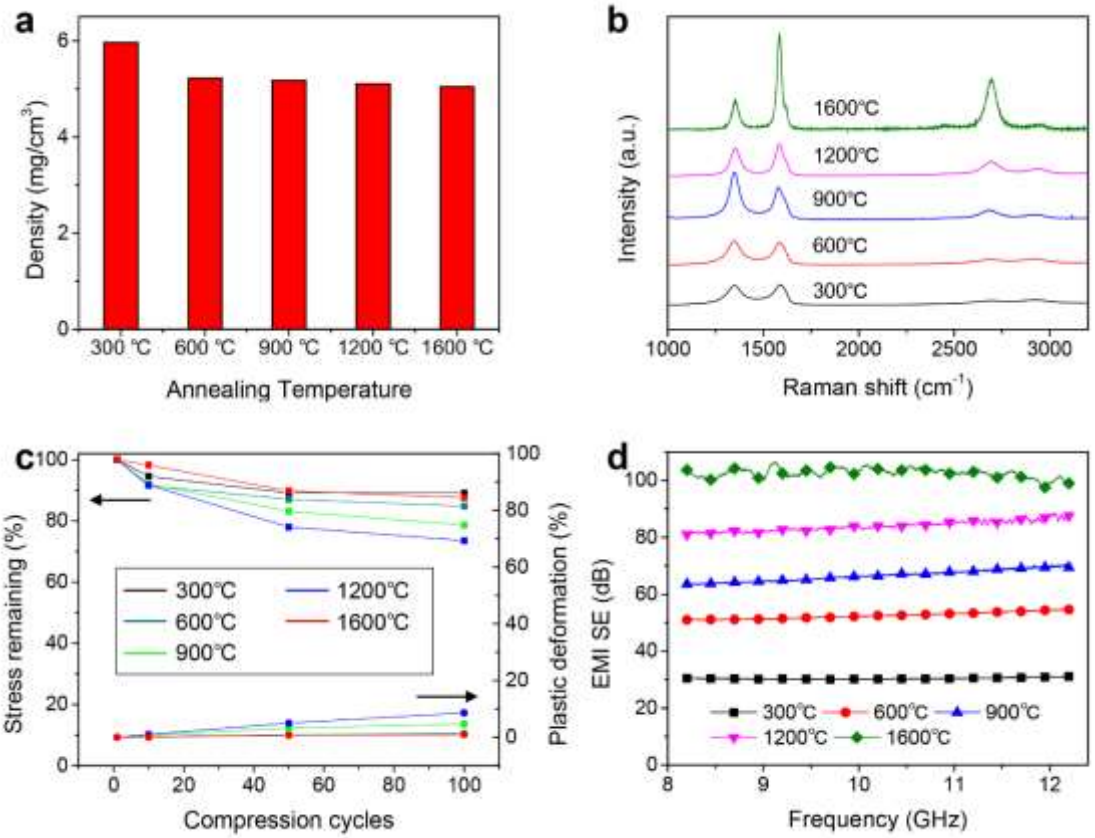

Figure S12 The density (a), Raman shift (b), stress remaining and plastic deformation (c), EMI SE (d) of HGA at different annealing temperature.

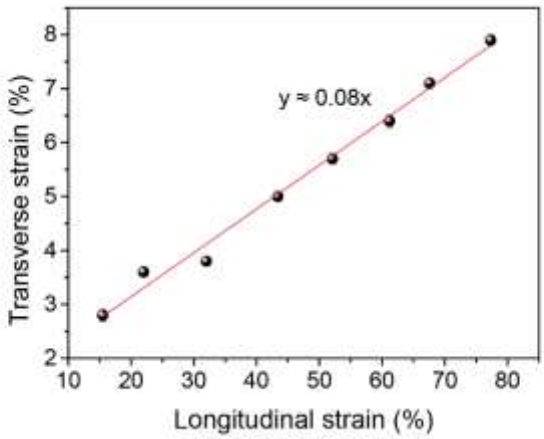

Figure S13 The transverse-longitudinal strain of HGA.

Figure S14 Digital camera image of HGA during twice folds.

Table S1 EMI shielding performance comparison of carbon-based materials and metal.

	Type	Density (mg/cm^3)	Thickness (mm)	EMI SE (dB)	SSE (dB/mm)	SSE/t ($dB\ cm^2/g$)
Foam	HGA (This work)	3.7	1	64.1 ±0.9	64.1	173243
		4.7	1	76.4 ±1.5	76.4	162553
		5.7	1	81.3 ±1.4	81.3	142631
		8.0	1	92.9 ±1.9	92.9	116125
		13.0	1	96.9 ±2.5	96.9	74538
	Carbon foam[1]	150	2	51.2	25.6	1706
	Carbon foam[2]	166	2	40	20	1205
	Carbon foam[3]	121	10	51	5.1	421
	Graphene aerogel[4]	12.5	2.5	43.29	17.3	17316
	rGO foam[5]	\	1.2	42	35	\
	Graphene aerogel[6]	5.5	2.5	20.4	8.2	14836
Composite	rGO/PEI[7]	300	2.3	12.8	5.6	186
	rGO/PS[8]	450	2	29	14.5	191.3
	rGO/PI[9]	22.4	0.8	21	26.2	11712
	SWCNT/PS[10]	561	1.2	18.5	15.4	275
	MWCNT/WPU[11]	39	1	21.1	21.1	5410
	rGO/PEI/Fe[12]	409	2.5	18	7.2	176
Film	Flexible graphite[13]	1121	0.127	57	449	4489
	Al foil[13]	2700	0.016	65	4063	15046
	Cu boil[14]	8960	0.01	70	7000	7812
	MXene film[14]	2390	0.008	57	7125	29811
	MXene film[14]	2310	0.01	92	9200	8850
	Graphene film[15]	1100	0.05	60	1200	10909
	CNT film[16]	2934	0.8	80	100	3408

Movie S1 The proceeding of vacuum bagging. It could be viewed online.

References

1 Zhang L, Liu M, Roy S, *et al*. Phthalonitrile-based carbon foam with high specific mechanical strength and superior electromagnetic interference shielding performance. ACS Appl Mater Interfaces, 2016, 8: 7422–7430.

2 Moglie F, Micheli D, Laurenzi S, *et al*. Electromagnetic shielding performance of carbon foams. Carbon, 2012, 50: 1972-1980.

3 Li YQ, Samad YA, Polychronopoulou K, *et al*. Lightweight and highly conductive aerogel-like carbon from sugarcane with superior mechanical and EMI shielding properties. ACS Sustain Chem Eng, 2015, 3: 1419–1427.

4 Li CB, Li YJ, Zhao Q, *et al*. Electromagnetic interference shielding of graphene aerogel with layered microstructure fabricated via mechanical compression. ACS Appl Mater Interfaces, 2020, 12: 30686-30694.

5 Umrao S, Gupta TK, Kumar S, *et al*. Microwave-assisted synthesis of boron and nitrogen co-doped reduced graphene oxide for the protection of electromagnetic radiation in Ku-band. ACS Appl Mater Interfaces, 2015, 7: 19831-19842.

6 Bi S, Zhang L, Mu C, *et al*. Electromagnetic interference shielding properties and mechanisms of chemically reduced graphene aerogels. Appl Surf Sci, 2017, 412: 529-536.

7 Ling J, Zhai W, Feng W, *et al*. Facile preparation of lightweight microcellular polyetherimide/graphene composite foams for electromagnetic interference shielding. ACS Appl Mater Interfaces, 2013, 5: 2677-2684.

8 Yan DX, Ren PG, Pang H, *et al*. Efficient electromagnetic interference shielding of lightweight graphene/polystyrene composite. J Mater Chem, 2012, 22: 18772-18774.

9 Li Y, Pei X, Shen B, *et al*. Polyimide/graphene composite foam sheets with ultrahigh thermostability for electromagnetic interference shielding. RSC Adv, 2015, 5: 24342-24351.

10 Yang Y, Gupta MC, Dudley KL, *et al*. Novel carbon nanotube-polystyrene foam composites for electromagnetic interference shielding. Nano Lett, 2005, 5: 2131-2134.

11 Zeng Z, Jin H, Chen M, *et al*. Lightweight and anisotropic porous MWCNT/WPU composites for ultrahigh performance electromagnetic interference shielding. Adv Funct Mater, 2016, 26: 303-310.

12 Shen B, Zhai W, Tao M, *et al*. Lightweight, multifunctional polyetherimide/graphene@Fe_3O_4 composite foams for shielding of electromagnetic pollution. ACS Appl Mater Interfaces, 2013, 5: 11383-11391.

13 Guan HT, Chung DDL. Absorption-dominant radio-wave attenuation loss of metals and graphite. J Mater Sci, 2021, 56: 8037-8047.

14 Shahzad F, Alhabeb M, Hatter C, *et al*. Electromagnetic interference shielding with 2D transition metal carbides (MXenes). Science, 2016, 353: 1137-1140.

15 Zhang L, Alvarez NT, Zhang M, *et al*. Preparation and characterization of graphene paper for electromagnetic interference shielding. Carbon, 2015, 82: 353-359.

16 Zeng Z, Chen M, Jin H, *et al*. Thin and flexible multi-walled carbon nanotube/waterborne polyurethane composites with high performance electromagnetic interference shielding. Carbon, 2016, 96: 768-777.